





Article

The Influence of NH_4NO_3 and NH_4ClO_4 on Porous Structure Development of Activated Carbons Produced from Furfuryl Alcohol

Agnieszka Kałamaga ^{1,*}, Maria Carmen Román-Martínez ², Maria Angeles Lillo-Ródenas ²
and Rafał Jan Wróbel ^{1,*}

¹ Department of Catalytic and Sorbent Materials Engineering, Faculty of Chemical Technology and Engineering, West Pomeranian University of Technology, Piastów 17 Ave., 70-310 Szczecin, Poland

² Department of Inorganic Chemistry, Materials Institute (IUMA), Faculty of Sciences, University of Alicante, Carretera de San Vicente del Raspeig s/n, 03690 Alicante, Spain

* Correspondence: agnieszka.kalamaga@zut.edu.pl (A.K.); rwrobel@zut.edu.pl (R.J.W.)

Abstract: The influence of NH_4NO_3 and NH_4ClO_4 on the porous texture and structure development of activated carbons produced from a non-porous polymeric precursor synthesized from furfuryl alcohol has been studied. The non-doped counterparts were prepared and studied for comparison purposes. NH_4NO_3 and NH_4ClO_4 -doped polymers were carbonized under N_2 atmosphere at 600 °C, followed by CO_2 activation at 1000 °C and the obtained carbon materials and activated carbons were thoroughly characterized. The porosity characterization data have shown that NH_4NO_3 -derived ACs present the highest specific surface area (up to 1523 m^2/g in the experimental conditions studied), and the resulting porosity distributions are strongly dependent on the activation conditions. Thus, 1 h activation is optimum for the microporosity development, whereas larger activation times lead to micropores enlargement and conversion into mesopores. The type of doping salts used also has a substantial impact on the surface chemical composition, i.e., C=O groups. Moreover, NH_4NO_3 and NH_4ClO_4 constitute good sources of nitrogen. The type and contribution of nitrogen species are dependent on the preparation conditions. Quaternary nitrogen only appears in doped samples prepared by carbonization and pyrrolic, pyridinic, and nitrogen oxide groups appear in the NH_4NO_3 -series. NH_4NO_3 incorporation has led to optimized materials towards CO_2 and C_2H_4 sorption with just 1 h activation time.

Keywords: activated carbons; carbonaceous materials; pore development; CO_2 adsorption; CO_2 uptake; supercapacitors; ethylene adsorption; furfuryl alcohol; hydrogen storage; methylene blue adsorption



Citation: Kałamaga, A.; Román-Martínez, M.C.; Lillo-Ródenas, M.A.; Wróbel, R.J. The Influence of NH_4NO_3 and NH_4ClO_4 on Porous Structure Development of Activated Carbons Produced from Furfuryl Alcohol. *Molecules* **2022**, *27*, 7860. <https://doi.org/10.3390/molecules27227860>

Academic Editors: Ines Matos, Maria Bernardo and Elena Perez Mayoral

Received: 18 October 2022

Accepted: 12 November 2022

Published: 14 November 2022

Publisher's Note: MDPI stays neutral with regard to jurisdictional claims in published maps and institutional affiliations.



Copyright: © 2022 by the authors. Licensee MDPI, Basel, Switzerland. This article is an open access article distributed under the terms and conditions of the Creative Commons Attribution (CC BY) license (<https://creativecommons.org/licenses/by/4.0/>).

1. Introduction

For several years, the main topic of researchers in activated carbons (ACs) has been developing porosity, which is one of the most important features of this type of material. The final porosity developed is often dependent on the used precursor. For the most part, activated carbons are produced from biomass like wood [1,2], stems [3], peels of fruits [4–6], or leaves [7]. Pores, which derive from the natural vascular system in this type of biomass precursors, are further developed in activated carbons obtained from them [8]. The second group of precursors is polymers, which are characterized by a non-porous structure and do not contain any impurities, such as silica or metal oxides, in their chemical composition [9,10]. Comparing these two kinds of precursors, it is claimed that biomass-derived activated carbons will have a more developed porous structure than polymer-derived carbonaceous materials because of the contained original pores in the former. Also, the less ordered structure of biomass precursors in comparison with polymeric ones explains that larger porosity usually developed in the former under comparable activation conditions [11]. However, in contrast to polymer precursors, biomass counterparts contain

mineral matter, which could act as a catalyst and accelerate the decomposition of the precursor during pyrolysis [12,13]. Additionally, the ashes derived from mineral matter could block pores and interfere with the adsorption processes [14,15]. Moreover, the presence of ash in carbonaceous materials can constitute a disadvantage in their different applications, e.g., in the production of carbon electrodes. Therefore, the choice of an appropriate precursor, with pure chemical composition and highly developed porous structure, could pose an issue. One solution to this problem is using furfuryl alcohol as a precursor in ACs production. Furfuryl alcohol is produced from biomass via its dehydration followed by catalytic hydrogenation of furfural [16–19]. A highly pure chemical composition is the result of repeated distillation/extraction processes. To sum up, it constitutes a promising precursor to activated carbons with high porosity and pure chemical composition. Moreover, using this type of precursor ash removal processes prior to activation could be omitted. This allows for the reduction of production costs and consumption of chemical reagents (i.e., HCl or distilled water) [20,21].

Currently, methods of porous texture development are divided into two groups: physical and the so-called chemical activation [22–28]. Physical activation is usually conducted under CO₂ or steam atmosphere at a temperature ranging from 800 °C to 1000 °C [29–31]. Rodriguez-Reinoso and co-workers reported that CO₂ activation leads to narrow micropores creation and, subsequently, their widening occurs [32]. In the case of steam, the widening of pores occurs from the early stages of activation. Apart from the conventional method of heating, porosity could be developed through unconventional heating methods, such as microwave or plasma treatment. In comparison to conventional heating, microwave heating is conducted under milder conditions such as lower temperatures, shorter processing times, and requires less energy [33,34]. Additionally, this method implies fewer requirements for feedstock pre-treatment. The main difference between conventional and microwave heating lies in their mechanism. In the case of conventional heating, a particle is heated from the external surface to the core, whereas in microwave heating, a particle is heated from the core to the external surface. The second unconventional method of pores creation is plasma treatment. Plasma could be created from the following gases: oxygen, nitrogen, argon, ammonia, or air [35–37]. In this method, the surface of the sample is bombarded with ions or free radicals. It leads to the breaking of sp² bonds in the carbon structure and the introduction of functional groups, which promote carbon etching. Inaccessible pores are opened and pore walls are collapsed. It causes an increase in porosity. Some advantages of plasma treatment include that it is faster than conventional heating and does not require solvents or toxic chemicals, being also highly efficient compared to chemical activation [35].

In the case of chemical activation methods, they are based on using mainly KOH, NaOH, K₂CO₃, H₃PO₄, or less frequently ZnCl₂ [6,34,38–53]. Additionally, in carbonaceous materials preparation, some researchers used the following chemical compounds: FeCl₂, NaCl, KCl, Fe₂(SO₄)₃, (Na[Al(OH)₄]), or NaSiO₃ [54,55]. Recently, researchers are also paying attention to the influence of ammonium nitrate (NH₄NO₃) on porosity development. Subramanian and Viswanathan prepared activated carbon from sucrose and ammonium nitrate by carbonization in the temperature range from 600 °C to 900 °C [56]. They reported that activation with ammonium nitrate caused an increase in porosity. Apart from that, they checked the impact of the sucrose/ammonium nitrate mass ratio on pores development. Based on TGA-DTG analysis, they noted that the addition of ammonium nitrate increases the stability of the sample. The highest mass loss was observed at 438–448 °C. Bayrak et al. produced carbonaceous materials from rice husks for Cr⁶⁺, Cu²⁺, and Ni²⁺ removal from water [57]. In their study, they used the following compounds as activating agents: NH₄Cl, NH₄Br, NH₄I, (NH₄)₂HPO₄, NH₄HCO₃ and NH₄NO₃. Comparing the mentioned compounds, ammonium nitrate caused the highest development of the porous structure. In contrast, the lowest impact on porosity was shown by ammonium iodide. Additionally, they noted that mesopores prevailed in activated carbons obtained by ammonium salts activation. Zheng and co-workers produced nitrogen/sulfur co-doped carbonaceous materials

for supercapacitors application [7]. In their study, they utilized ginkgo leaves as precursors and examined the influence of ammonium nitrate on porous structure development. Additionally, they described the decomposition of ammonium nitrate, which takes place at temperatures over 220 °C. The authors claimed that activation is a redox reaction, and as a result of the increase of the heat-treatment temperature, ammonium nitrate is melted and partially decomposed to $\text{HNO}_{3(g)}$, $\text{NH}_{3(g)}$, N_2O , and $\text{H}_2\text{O}_{(g)}$. Simultaneously, the oxidation reaction of biomass-derived carbon takes place. Gaseous products, such as CO_2 , H_2O , NO_2 , and N_2O , swell in graphene sheet-like carbon and further promote porous structure creation. In Table 1, specific surface areas of activated carbons obtained by ammonium nitrate activation are compiled.

Table 1. Comparison of the specific surface area of activated carbons obtained through ammonium nitrate activation.

Sample	Preparation Parameters	Specific Surface Area [m ² /g]	Ref.
C _{NA900}	Sucrose/ NH_4NO_3 mass ratio 3:1 (C _{NA900}) and 2:1 (C _{NB900}). Carbonization under N_2 atmosphere for 6 h at 900 °C.	489	[56]
C _{NB900}		518	
AC_ NH_4NO_3	Rice husk/ NH_4NO_3 mass ratio: 1:4 Carbonization under $\text{N}_{2.5}$ atmosphere for 0.5h at 600 °C.	457	[57]
AN/GL ₇₀₀	Ginkgo leaves/ NH_4NO_3 mass ratio: 1:2. Carbonization under $\text{N}_{2.5}$ atmosphere for 1 h at 700 °C.	672	[7]
PWAC	Pistachio wood wastes/ NH_4NO_3 impregnation ratio: 5% wt. Pyrolysis under N_2 atmosphere at 800 °C for 2 h.	1448	[58]
N-carbon ₇₀₀	Cellulose/ NH_4NO_3 /distilled water mass ratio 1:1:10. Hydrothermal carbonization at 240 °C for 5 h. Activation with KOH at 700 °C and 800 °C for 1 h.	1184	[59]
N-carbon ₈₀₀		1976	

As shown in the table above, all the activated carbons were prepared via chemical activation of biomass, in which original pores exist. Based on the literature, among the utilized chemical compounds containing NH_4^+ , the ammonium nitrate ion has the highest impact on pores development. To the best of our knowledge, there are no scientific reports about ammonium perchlorate (NH_4ClO_4), which is also a strong oxidant. In industry, NH_4ClO_4 is commonly utilized as a solid rocket propellant. NH_4ClO_4 starts to decompose at 130 °C, and the main decomposition products include steam, nitrogen, oxygen, and chlorine [60,61]. From an environmental point of view, the produced chlorine leads to ozone layer degradation. For this reason, the produced chlorine should be adsorbed and utilized in other processes, such as in water disinfection tasks [62].

Taking all this into account, the general objectives of this study are to compare and examine the influence of ammonium nitrate and ammonium perchlorate on the preparation of activated carbon, paying attention to properties such as pore volume and distribution, specific surface area, size of crystallites and chemical composition. These carbonaceous materials will be prepared from furfuryl alcohol. Therefore, the impact of any silica and metal oxides, present in other precursors, on pore creation will be eliminated. The potential application of the obtained materials will be the adsorption of gases. Therefore, carbon dioxide (CO_2) and ethylene (C_2H_4) will be used as model gases. Both gases negatively affect the environment. CO_2 is one of the greenhouse gases whose emission is still increasing [63]. Currently, the concentration of CO_2 in the atmosphere is 415 ppm. It mainly comes from anthropogenic sources, such as fossil fuel combustion or cement production. The high concentration of CO_2 intensifies the greenhouse effect, which results in various climatic disasters, for example, droughts, melting of glaciers, and forest fires. C_2H_4 is known to be a plant hormone, which controls the ripening processes [64]. It is produced during the putrefactive processes of plants and leads to the faster ripening of vegetables that are nearby. For this reason, the regulation of the concentration of C_2H_4 is especially important in the case of vegetable and fruit storage in the food industry. Note that these selected

molecules differ in their kinetic diameters. They are 0.33 nm and 0.39 nm for CO₂ and C₂H₄, respectively.

2. Materials and Methods

2.1. Materials

In this study, the preparation scheme can be summarized as follows: either a mixture of furfuryl alcohol, maleic acid, and ethylene glycol (Mixture 1) or a mixture of furfuryl alcohol, maleic acid, and ethylene glycol with either NH₄NO₃ or NH₄ClO₄ (Mixture 2) led to polymeric materials, that were carbonized in a nitrogen atmosphere at 600 °C. The derived materials were characterized as obtained, and also after their activation with CO₂ at 1000 °C for different holding times.

The samples obtained after carbonization were named AC in the Mixture 1 scheme, or either AC_NH₄NO₃ or AC_NH₄ClO₄ in the Mixture 2 carbonization scheme. Note that in the case of Mixture 2, this “carbonization” can really imply some chemical activation as well. Additionally, these materials were submitted to activation by CO₂. In this case, their nomenclature includes a number representing the holding time of the CO₂ activation step (in hours). A detailed description of the preparation scheme is shown next.

An activation precursor was prepared from 15 mL furfuryl alcohol (Nr. CAS: 98-00-0, Sigma Aldrich), 2 g maleic acid (Nr. CAS: 110-16-7, Chempur), and 14 mL ethylene glycol (Nr. CAS: 107-21-1, EUROCHEM). All reagents were mixed on the magnetic stirrer for 30 min at ambient temperature. Afterward, the mixture was heated in an oven from 40 °C to 200 °C. It was held for 10 min at 40 °C, 50 °C, 80 °C, and for 18 h at 200 °C. After heating, the obtained polymeric precursor was cooled at an ambient temperature and ground.

In the case of chemically activated materials, NH₄NO₃ (Nr. CAS: 6484-52-2, Chempur) or NH₄ClO₄ (prepared from ammonia water (Nr. CAS: 1336-21-6, STANLAB) and perchloric acid (Nr. CAS: 7601-90-3, Chempur)) salts were firstly dissolved in 14 mL ethylene glycol. An amount of 1 g NH₄NO₃ or 1 g NH₄ClO₄ was added. After that, the solutions were added to the furfuryl alcohol and maleic acid mixture (same quantities as in the previous conditions). All reagents were mixed on the magnetic stirrer for 30 min at an ambient temperature. Afterward, the mixture was heated in an oven from 40 °C to 200 °C. It was held for 10 min at 40 °C, 50 °C, 80 °C, and for 18h at 200 °C. After heating, each obtained precursor polymer was cooled at an ambient temperature and ground.

The three different precursors (either prepared with NH₄NO₃, NH₄ClO₄, or without any of those) were subjected to a carbonization process under N₂ atmosphere at 600 °C (temperature ramp 5 °C/min) for 4 h in an electric tube furnace (STF 15/180, Carbolite Gero). The flow of N₂ was 100 mL/min. The three obtained materials were characterized as obtained and also submitted to a next step. In it, 1 g of each resulting sample was activated under CO₂ atmosphere at 1000 °C (temperature ramp 5 °C/min) for 1 h, 2 h, or 3 h. The flow of CO₂ was 50 mL/min during the whole process.

For simplicity, in some parts of the discussion these three sets of samples are referred to as “unmodified”, “NH₄NO₃ modified”, or “NH₄ClO₄ modified”.

The purity of N₂ and CO₂ were 5.0 and 4.5, respectively. Both gases were provided by Messer.

2.2. Methods

The porous structure of the obtained activated carbons was characterized using volumetric analysis (Autosorb, Quantachrome; Boynton Beach, USA). Pore volume and pore size distribution were determined based on N₂ adsorption/desorption isotherms at −196 °C using the QSDFT model. Specific surface areas were calculated from the BET equation applied to the N₂ adsorption data. Additionally, adsorption of CO₂ at 0 °C allowed to determine the pores with diameters lower than 1.0 nm. In this case, the pore size distribution was determined using the NLDFT model. The porosity characterization data were calculated using QuadraWin software.

The structural properties of the ACs were analyzed using X-ray powder diffraction (Empyrean, PANalytical; Malvern, UK). Measurements were conducted in the 5° – 80° 2θ range using copper radiation ($K_{\alpha} = 0.154056$ nm). HighScore Plus software was used for XRD patterns interpretation and for stacking height (Lc) and lateral size (La) calculation.

Disorder degrees in the ACs were estimated using Raman spectroscopy analysis (Jasco NRS-5100; Easton, USA). Measurements were carried out with an Ar laser (wavelength = 532.11 nm, power = 2.0 mW, magnification of the objective = 20x). The activated carbons were scanned from 70 cm^{-1} to 3780 cm^{-1} .

X-ray photoelectron spectroscopy was used to confirm the surface chemical composition of the carbons (PREVAC; Rogów, Poland). Functional groups were determined based on C 1s, O 1s, and N 1s signals. Data were calculated using CasaXPS 2.3.16 software.

Thermal stabilities of the carbonaceous materials were determined using a thermobalance (NETZSCH, STA 449F5; Selb, Germany). An amount of 10 mg of sample was heated from 50°C to 950°C with a temperature ramp of $20^{\circ}\text{C}/\text{min}$. Measurements were conducted both under an argon or oxygen atmosphere. The flow of gases was $30\text{ mL}/\text{min}$ or $50\text{ mL}/\text{min}$, respectively.

To test the ACs in their final application, adsorption measurements of CO_2 and C_2H_4 were conducted on a homemade thermobalance operating under 1025 hPa. Firstly, 0.4 g of AC sample was heated to 250°C to remove adsorbed compounds and moisture. The sample was held for 10 min at this temperature. After that, it was cooled to 30°C under the investigated gas atmosphere. The flow of CO_2 and C_2H_4 was $40\text{ mL}/\text{min}$. Sorption capacities were calculated based on the mass difference between 250°C and 30°C .

3. Results and Discussion

3.1. Porous Structure

3.1.1. N_2 Adsorption at -196°C

N_2 adsorption/desorption isotherms are presented in Figure 1.

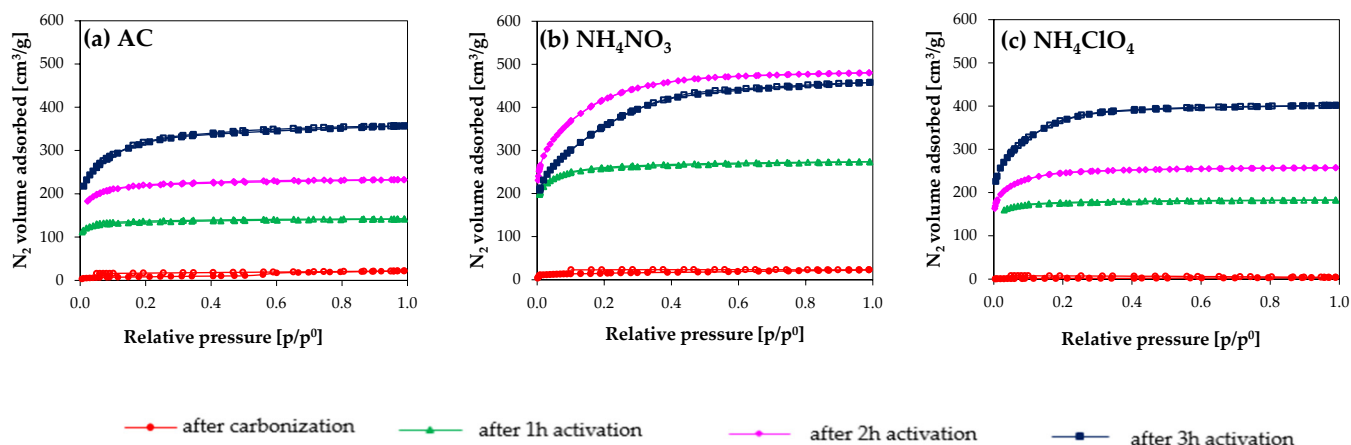


Figure 1. N_2 adsorption/desorption isotherms at -196°C of samples: (a) AC series, (b) NH_4NO_3 series, and (c) NH_4ClO_4 series.

Figure 1 shows that the carbonization of the three different precursors leads to a very similar and poor porosity. Hence, the discussion is focused on data from samples after CO_2 activation. According with the IUPAC classification, the obtained isotherms (Figure 1) are type I (b) [65]. They are characteristic of materials having wide micropores and narrow mesopores ($< \sim 2.5$ nm). In this case, N_2 adsorption is enhanced in the NH_4ClO_4 series and, especially, in the NH_4NO_3 series: comparing the influence of NH_4NO_3 and NH_4ClO_4 on N_2 adsorption it can be seen that higher N_2 adsorption was achieved in the NH_4NO_3 -derived carbons.

Focusing on NH_4NO_3 , larger N_2 adsorption was observed in $\text{AC_NH}_4\text{NO}_3\text{_{2h}}$ in comparison to sample $\text{AC_NH}_4\text{NO}_3\text{_{3h}}$, and also their porosity distributions were noticeably

different. This was not observed in the AC and NH_4ClO_4 -modified samples (carbonized in N_2 and activated with CO_2). The comparison between these two series highlights that the activation reaction in the NH_4NO_3 series proceeds in a much more efficient way than in the NH_4ClO_4 one. From a certain activation time (i.e., 3 h), a noticeable porosity widening is noticed in the NH_4NO_3 series, and even some porosity destruction, so the selection of the activation time is very important. The impact of activating salts on pore size distributions is presented in Figure 2.

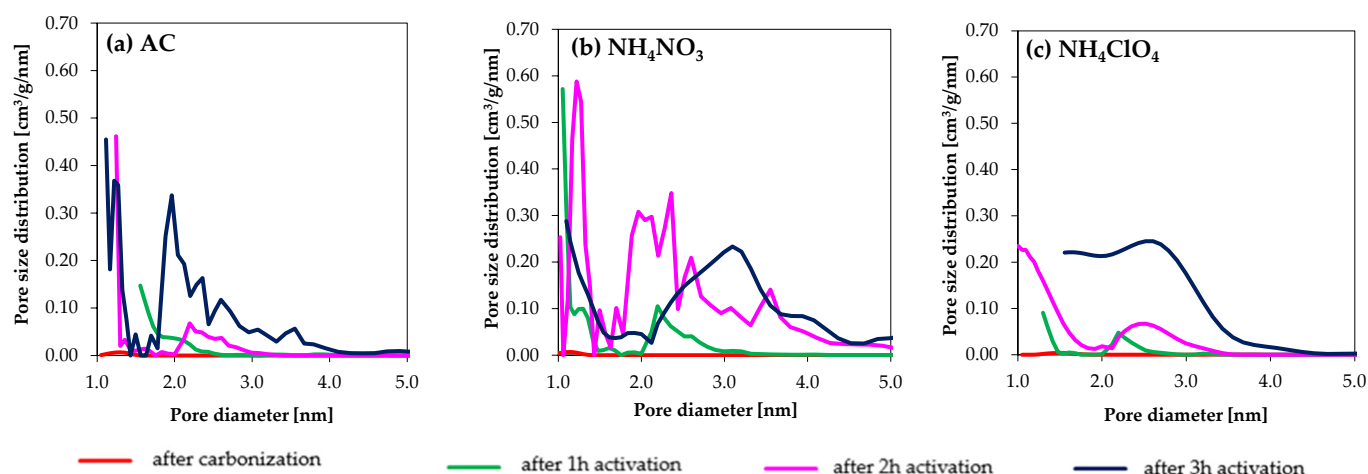


Figure 2. Pore size distribution of samples (a) AC series, (b) NH_4NO_3 series, (c) NH_4ClO_4 series calculated from N_2 adsorption data at -196°C .

This figure confirms that differences in the pore size distributions are noted for the three series of samples and, in general, the larger activation times lead to larger porosities.

In the ACs series, the highest porosity was reached in the sample AC_3h, whose mean pore size is around 2.0 nm. The mean pore size for NH_4ClO_4 _3h is around 2.5 nm, whereas it reaches 3.0 nm for NH_4NO_3 _3h.

Although higher pore volumes are in general present in the NH_4NO_3 series in comparison with the NH_4ClO_4 one, these differences minimize for 3 h activation time.

In Table 2, specific surface areas and pore volumes calculated from N_2 adsorption data are presented.

Table 2. Specific surface areas and pores volume in the obtained activated carbons.

Sample	SSA ¹ [m ² /g]	V _{total} [cm ³ /g]	V _{micro} ² [cm ³ /g]	V _{meso} ³ [cm ³ /g]
AC	28	0.03	0.00	0.03
AC_1h	535	0.22	0.19	0.01
AC_2h	843	0.36	0.30	0.03
AC_3h	1174	0.55	0.36	0.15
AC_ NH_4NO_3	57	0.04	0.02	0.02
AC_ NH_4NO_3 _1h	999	0.43	0.34	0.04
AC_ NH_4NO_3 _2h	1523	0.75	0.41	0.28
AC_ NH_4NO_3 _3h	1292	0.71	0.26	0.39
AC_ NH_4ClO_4	6	0.01	0.00	0.00
AC_ NH_4ClO_4 _1h	696	0.28	0.24	0.02
AC_ NH_4ClO_4 _2h	933	0.40	0.27	0.09
AC_ NH_4ClO_4 _3h	1342	0.62	0.29	0.26

¹ SSA—The specific surface area, calculated by the BET equation. ² V_{micro}—The volume of pores with diameter lower than 2 nm, determined from N_2 adsorption. ³ V_{meso}—The volume of pores with diameter in the range from 2 nm to 50 nm, estimated from N_2 adsorption.

This table shows that carbons obtained only through the “carbonization” process in N_2 at $600\text{ }^\circ\text{C}$ are characterized by low specific surface areas. In the case of AC, this sample is indeed obtained by carbonization. In $AC_NH_4NO_3$ and $AC_NH_4ClO_4$, some chemical activation may occur as well (due to the chemical compounds incorporated during the preparation of the precursor). This is especially remarkable in the $AC_NH_4NO_3$ sample, and explains the $57\text{ m}^2/\text{g}$ of surface area reached.

The porosity values in $AC_NH_4NO_3$ and $AC_NH_4ClO_4$ series are lower than, for example, those reported by Bayrak and co-workers, who used rice husks as precursors [57]. Although the activation temperature is the same in both cases, the higher specific surface areas reported by Bayrak et al. may be very much influenced by the different nature of the precursor.

Sample $AC_NH_4NO_3_2\text{h}$ reached the highest BET specific surface area ($1523\text{ m}^2/\text{g}$) and the highest volume of micropores ($0.41\text{ cm}^3/\text{g}$). After the extension of the activation time to 3 h, the volume of micropores decreased by half and the mesopore volume increased. In the case of the NH_4ClO_4 series, the highest specific surface area and pores volume was exhibited by sample $AC_NH_4ClO_4_3\text{h}$ ($1342\text{ m}^2/\text{g}$ and $0.29\text{ cm}^3/\text{g}$, respectively). Comparing the effect of NH_4NO_3 and NH_4ClO_4 , it has been found that NH_4NO_3 is more efficient for porosity development.

It is difficult to compare the ACs produced in the present study with those from other papers. For example, Mu et al. produced activated carbons by hydrothermal method followed by KOH activation at $800\text{ }^\circ\text{C}$ for 1 h [59]. The highest specific surface area reached was $1976\text{ m}^2/\text{g}$. It must be noted that so-developed porous structure is partially related to using KOH, one of the most effective activating agents, but also the proportion of chemical agent needs to be taken into consideration.

3.1.2. CO_2 Adsorption at $0\text{ }^\circ\text{C}$

Figure 3 presents the CO_2 adsorption isotherms at $0\text{ }^\circ\text{C}$ for the different samples, which shows, that, in general, CO_2 adsorption is lowest for the carbonized samples, whereas those activated for 1 h activation show the highest CO_2 adsorption. Increasing the activation time beyond 1 h leads to a decrease in the narrow micropores (characterized by CO_2 adsorption), being such a decrease is especially remarkable for $NH_4NO_3_3\text{h}$. The similarity in the AC and NH_4ClO_4 series remarks that no benefit, from the point of view of narrow micropore development, occurs by incorporating this chemical agent into the composition of the precursor, and only $NH_4NO_3_1\text{h}$ is interesting from that point of view.

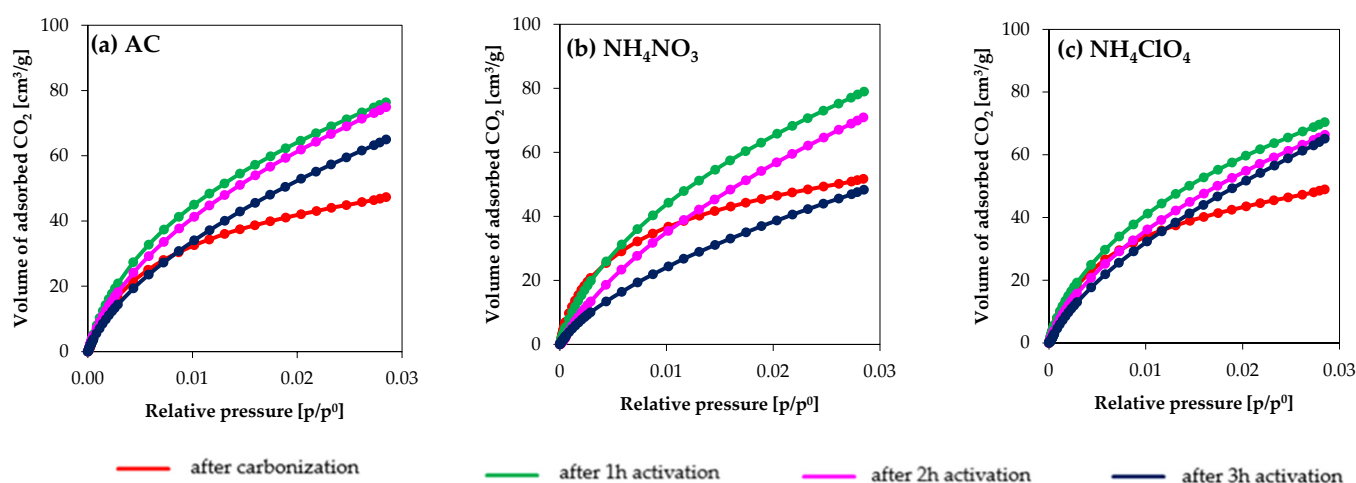


Figure 3. CO_2 adsorption/desorption isotherms at $0\text{ }^\circ\text{C}$ for (a) AC series, (b) NH_4NO_3 series, (c) NH_4ClO_4 series.

Figure 4 highlights that from the point of view of the CO_2 pore size distributions, there are no important differences between the series. More remarkably, in the just-carbonized carbons, there is an increase in the volume of pores in the diameter range from 0.3 nm to 0.7

for AC_NH₄NO₃ and AC_NH₄ClO₄. After activation, micropore size distributions were comparable for all the obtained samples and the differences between them were negligible.

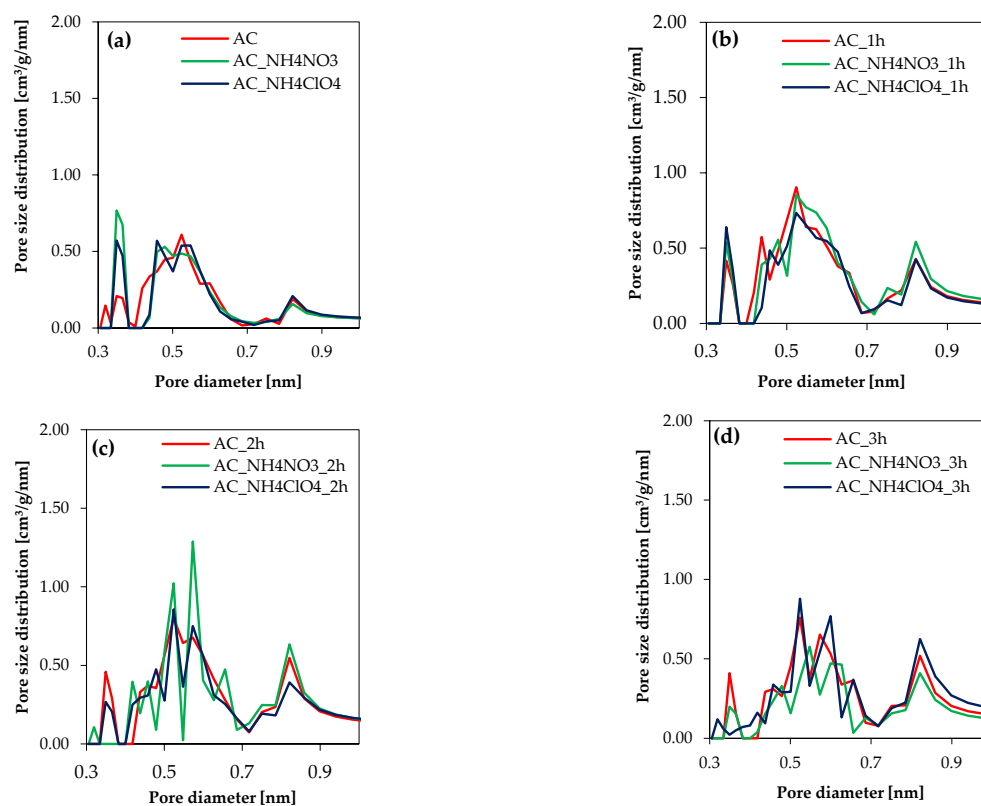


Figure 4. Micropore size distributions based on CO₂ adsorption data at 0 °C for (a) just-carbonized carbons, (b) activated carbons after 1 h activation, (c) activated carbons after 2 h activation, (d) activated carbons after 3 h activation.

Micropore specific surface areas and micropores volumes determined by CO₂ adsorption at 0 °C are presented in Table 3.

Table 3. CO₂ micropore specific surface areas and micropore volumes for the prepared ACs.

Sample	CO ₂ Micropore Specific Surface Area ¹ [m ² /g]	V _{total} [cm ³ /g]	V _{0.7 nm} ² [cm ³ /g]	V _{0.8 nm} ³ [cm ³ /g]	V _{1.0 nm} ⁴ [cm ³ /g]
AC	454	0.15	0.10	0.10	0.12
AC_1h	706	0.27	0.15	0.16	0.21
AC_2h	686	0.27	0.14	0.16	0.21
AC_3h	589	0.25	0.12	0.14	0.19
AC_NH ₄ NO ₃	496	0.16	0.11	0.11	0.13
AC_NH ₄ NO ₃ _1h	724	0.29	0.15	0.17	0.22
AC_NH ₄ NO ₃ _2h	640	0.27	0.13	0.15	0.21
AC_NH ₄ NO ₃ _3h	435	0.19	0.09	0.10	0.14
AC_NH ₄ ClO ₄	471	0.15	0.10	0.10	0.13
AC_NH ₄ ClO ₄ _1h	651	0.25	0.14	0.15	0.19
AC_NH ₄ ClO ₄ _2h	600	0.25	0.13	0.14	0.19
AC_NH ₄ ClO ₄ _3h	587	0.27	0.11	0.13	0.20

¹ SSA_{CO₂}—The micropore specific surface area obtained on the basis on CO₂ adsorption at 0 °C. ² V_{0.7 nm}—The volume of pores with diameter up to 0.7 nm., determined from CO₂ adsorption. ³ V_{0.8 nm}—The volume of pores with diameter up to 0.8 nm., determined from CO₂ adsorption. ⁴ V_{1.0 nm}—The volume of pores with diameter up to 1.0 nm., determined from CO₂ adsorption.

Table 3 confirms that the addition of oxidizing salts to the composition of the precursors caused insignificant changes in the narrow microporous structure: comparing the AC, NH_4NO_3 , and NH_4ClO_4 series, noticeable differences were not observed. The highest microporous specific surface area and micropores volume were exhibited by the sample AC_ NH_4NO_3 _1h. They were $724 \text{ m}^2/\text{g}$ and $0.29 \text{ cm}^3/\text{g}$, respectively.

3.2. Structural Properties

3.2.1. X-ray Diffraction Analysis

XRD patterns for all obtained activated carbons are presented in Figure 5. They present two main reflections at positions 24° and 45° . Their Miller indexes are (002) and (10), respectively [66].

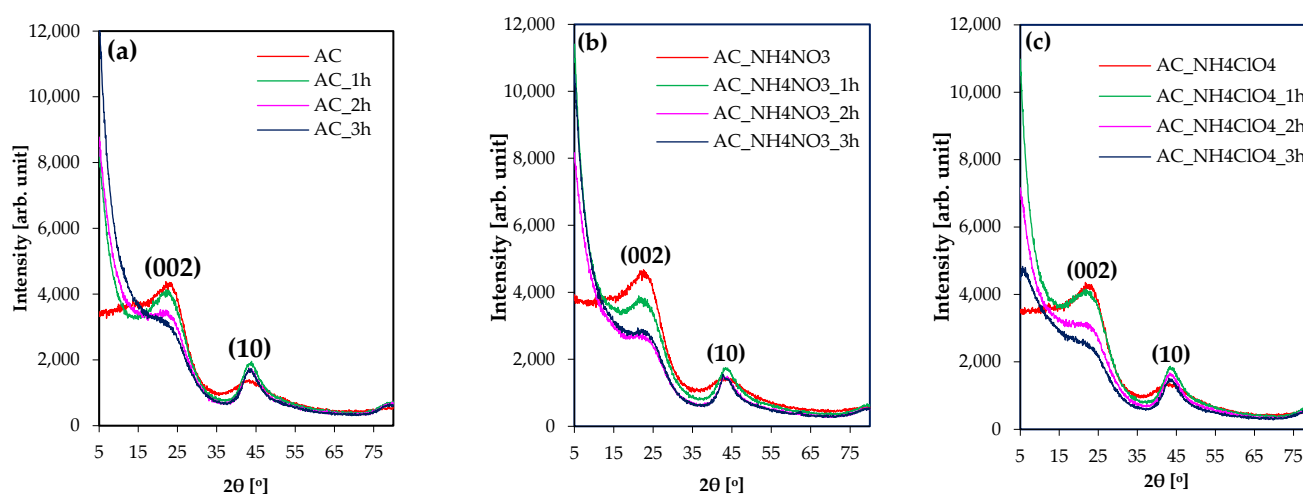


Figure 5. XRD-patterns of (a) AC series, (b) NH_4NO_3 series, (c) NH_4ClO_4 series.

In the case of just-carbonized carbons, peaks for (002) reflection, which corresponds to the spacing between graphenic planes, are high and wide. Activation processes lead to their intensity decreasing and peak narrowing with the extension of the activation time. A more pronounced (002) reflection decrease (i.e., for 3 h activation time with respect to the carbonized sample) is observed in the NH_4NO_3 series in comparison to AC and NH_4ClO_4 ones.

For all the obtained just-carbonized samples, (10) reflections are broad and smooth. The position of (10) reflections is changing with the lateral size of carbon pieces. This feature, and the origin of (10) reflection are very well described in detail elsewhere [66,67].

1 h activation processes led to the increase of the intensity of peaks corresponding to those reflections, becoming narrower and sharper. Moreover, the extension of the activation time caused a slight decrease in the intensity of the peaks associated to the (10) reflections.

Based on obtained XRD patterns, stacking height (L_c) and lateral size (L_a) of carbon crystallites were calculated from the following equations:

$$L_c = \frac{0.89\lambda}{B_c \cos\theta_c} \quad (1)$$

$$L_a = \frac{1.89\lambda}{B_a \cos\theta_a} \quad (2)$$

where θ is the angle of a reflection, λ is wavelength of X-rays, and B_c and B_a are full widths at half maximum (FWHM) of (002) and (10) reflections, respectively.

Stacking height (L_c), lateral size (L_a) and interlayer distance (d_{002}) of carbon crystallites are presented in Table 4.

Table 4. Stacking height (Lc), lateral size (La) and interlayer distance (d_{002}) of carbon crystallites.

Sample	Lc [nm]	La [nm]	d_{002} [nm]
AC	1.0	1.9	0.381
AC_1h	0.9	3.1	0.392
AC_2h	1.1	3.2	0.387
AC_3h	0.9	3.2	0.388
AC_NH ₄ NO ₃	0.9	1.9	0.394
AC_NH ₄ NO ₃ _1h	1.1	3.1	0.381
AC_NH ₄ NO ₃ _2h	1.2	3.3	0.373
AC_NH ₄ NO ₃ _3h	1.2	3.5	0.371
AC_NH ₄ ClO ₄	0.7	1.9	0.417
AC_NH ₄ ClO ₄ _1h	1.0	3.1	0.388
AC_NH ₄ ClO ₄ _2h	1.0	3.3	0.387
AC_NH ₄ ClO ₄ _3h	1.1	3.3	0.384

These data show that modification of the parent polymers with the NH₄NO₃ or NH₄ClO₄ salts caused substantial changes in the stacking height of carbon crystallites during the carbonization process, whereas the lateral size was not affected. In comparison with AC, AC_NH₄ClO₄ shows a decrease in stacking height from 1.0 nm to 0.7 nm. In the case of AC_NH₄NO₃, this difference was only 0.1 nm.

After the activation processes, the lateral size significantly increased, whereas the stacking height increased only slightly. Sample AC_NH₄NO₃_3h exhibited the highest value of Lc and La. They were 1.2 nm and 3.5 nm, respectively. The same material presented the highest volume of mesopores (0.39 cm³/g). In the case of sample AC_NH₄NO₃_2h, which has the highest specific surface area, Lc and La values are 1.2 nm and 3.3 nm, respectively. Therefore, an increase of lateral size could also be related to the development of porosity.

3.2.2. Raman Spectroscopy

The ordered and defective carbon structures in the carbonaceous materials were estimated on the basis of the intensity ratio of D-band to G-band (I_D/I_G). The formation of the D-band appears near 1345 cm⁻¹ and is related to disordered structure. On the other hand, the G-band is associated with the regular structure of carbon and appears near 1596 cm⁻¹. The crystallites size (La) [68–70] were determined based on the following equation, and are compiled in Table 5:

$$La = \frac{C}{R} \quad (3)$$

where R is the I_D/I_G intensity ratio of D-band to G-band and constant C is 35 in this study.

The carbonized samples prepared with the doped polymers show a higher disordered structure than the one prepared with the undoped polymer. Comparing the influence of the type of salts, it can be noted that carbons from the NH₄NO₃ series are characterized by a more disordered structure than those from NH₄ClO₄ series. After the activation processes, the disordered structure significantly increased. The highest increase in I_D/I_G ratio was exhibited after 3 h activation by all the obtained samples. The I_D/I_G ratio for them was 1.09.

The largest size of crystallites (La) was exhibited by the sample AC. It was 5.9 nm. Significantly lower La values were exhibited by the carbonized samples from NH₄NO₃ and NH₄ClO₄ series. They were 4.9 nm and 5.1 nm, respectively. Further activation processes caused a decrease in the size of carbon crystallites. Moreover, this results in similar sizes of crystallites. The lowest carbon crystallites were exhibited by all the samples after 3 h activation.

The structural parameters La obtained by Raman are in good agreement with La determined by the XRD method.

Table 5. I_D/I_G ratios and carbon crystallites (L_a) size of obtained activated carbons.

Sample	I_D/I_G Ratio	D-Band Width [cm^{-1}]	G-Band Width [cm^{-1}]	L_a [nm]
AC	0.60	272.81	77.48	5.9
AC_NH ₄ NO ₃	0.71	283.99	85.86	4.9
AC_NH ₄ ClO ₄	0.68	256.92	96.28	5.1
AC_1h	1.09	194.63	93.65	3.2
AC_NH ₄ NO ₃ _1h	0.93	220.33	94.07	3.8
AC_NH ₄ ClO ₄ _1h	0.97	212.37	94.17	3.6
AC_2h	1.03	169.21	81.10	3.4
AC_NH ₄ NO ₃ _2h	1.01	202.89	91.47	3.5
AC_NH ₄ ClO ₄ _2h	0.95	201.71	90.14	3.7
AC_3h	1.09	179.18	83.17	3.2
AC_NH ₄ NO ₃ _3h	1.09	191.59	87.11	3.2
AC_NH ₄ ClO ₄ _3h	1.09	193.59	89.99	3.2

3.3. Surface Chemical Composition

Table 6 summarizes the surface composition of the prepared ACs, determined by XPS analysis. Hydrogen is also present in the chemical composition of the ACs, but it cannot be detected by XPS.

Table 6. Surface chemical composition, determined using XPS, for the obtained activated carbons.

Sample	Concentration [at. %]		
	C	O	N
AC	87	13	0
AC_1h	97	3	0
AC_2h	97	3	0
AC_3h	96	4	0
AC_NH ₄ NO ₃	88	9	3
AC_NH ₄ NO ₃ _1h	91	6	3
AC_NH ₄ NO ₃ _2h	89	8	3
AC_NH ₄ NO ₃ _3h	87	9	4
AC_NH ₄ ClO ₄	90	7	3
AC_NH ₄ ClO ₄ _1h	91	8	2
AC_NH ₄ ClO ₄ _2h	90	8	2
AC_NH ₄ ClO ₄ _3h	85	13	3

Based on the surface chemical composition analysis by XPS, it can be noted that the preparation of ACs with this procedure, which includes the precursor ‘doping’ with NH₄NO₃ or NH₄ClO₄, is suitable for the incorporation of nitrogen heteroatoms in the composition of the ACs. Thus, the corresponding NH₄NO₃ and NH₄ClO₄-ACs contain 2–4 at. % of nitrogen on their surface and the concentrations of nitrogen are similar for both NH₄NO₃ and NH₄ClO₄ series.

These ACs also possess noticeable surface oxygen contents. The highest concentration of oxygen was exhibited by the sample named AC. Comparing the just-carbonized NH₄NO₃ and NH₄ClO₄ series, it can be observed that sample AC_NH₄NO₃ has a higher concentration of oxygen than AC_NH₄ClO₄. Further activation of the NH₄NO₃ series leads to lower oxygen concentration than in the case of the NH₄ClO₄ series. Chlorine is not detected in the AC_NH₄ClO₄ obtained materials. It is assumed that it was removed as a gaseous byproduct during the carbonization process.

The XPS signals of carbon, oxygen, and nitrogen have allowed determining the type and the concentration of functional groups appearing on the surface of the obtained activated carbons. They are presented in Figure 6.

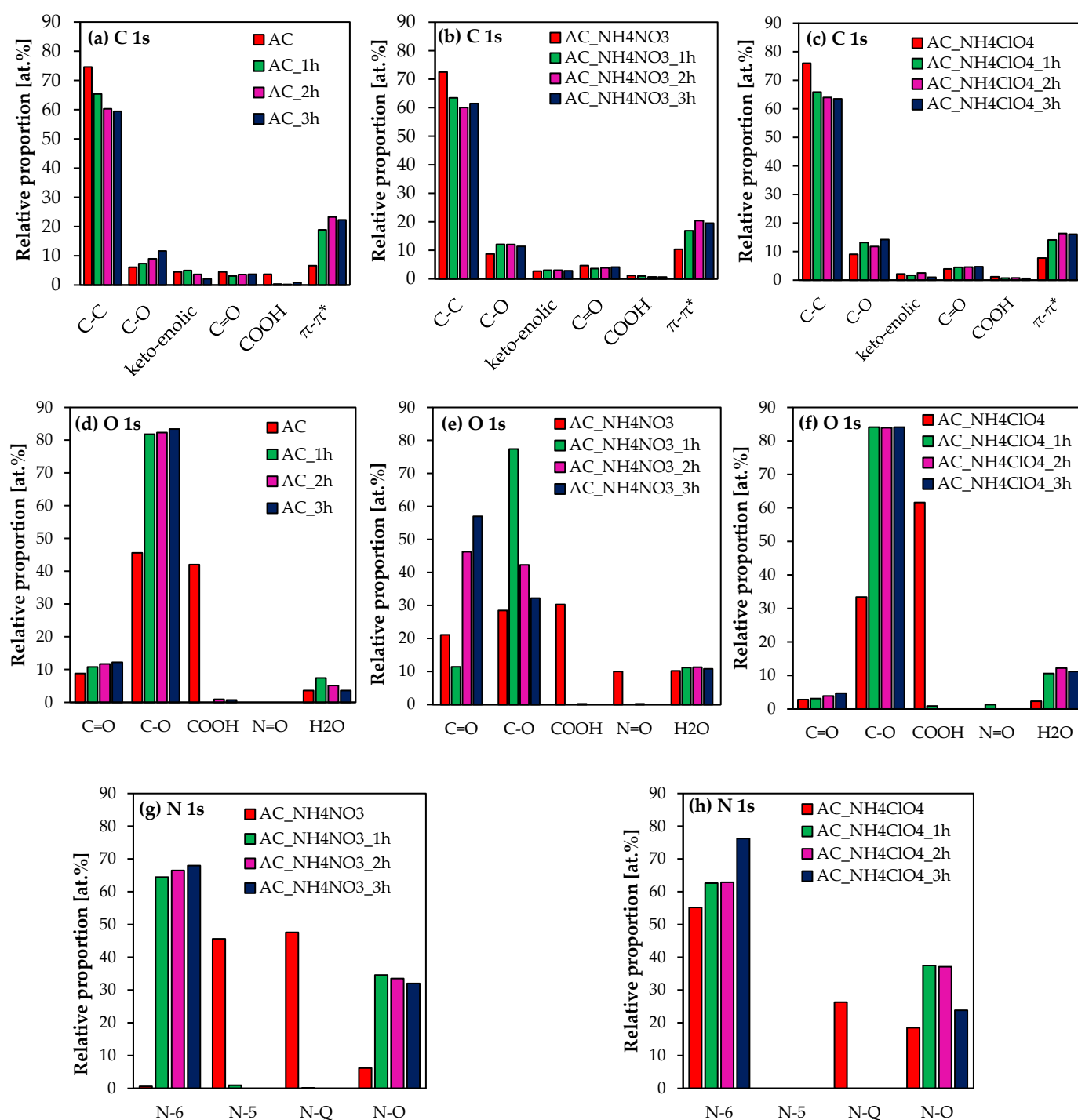


Figure 6. Carbon functional groups (a–c), oxygen functional groups (d–f), nitrogen functional groups (g,h) on the surface of the obtained activated carbons.

Functional groups containing carbon were identified based on the following binding energies: C-C 284.6 ± 0.3 eV, C-O 286.1 ± 0.3 eV, keto-enolic 286.4 ± 0.3 eV, C=O 287.6 ± 0.3 eV, COOH 289.1 ± 0.3 eV and π - π^* (satellite peak of carbon in aromatic compounds, C-C with sp^2 hybridization) 292.15 ± 2.15 eV. The full width at half maximum (FWHM) was set at the same value for each functional group, except for the satellite peak. In the case of O 1s signal, binding energies for particular components were: C=O 531.1 ± 0.3 eV, C-O 532.8 ± 0.3 eV, COOH 534.2 ± 0.3 eV, N=O 535.2 ± 0.3 eV, and gas phase H₂O 536.1 ± 0.3 eV. Nitrogen functional groups were determined based on the

following binding energies: pyridinic N-6 397.8 ± 0.3 eV, pyrrolic N-5 399.9 ± 0.3 eV, quaternary N-Q 401.2 ± 0.3 eV, and nitrogen oxides N-O 402.2 ± 0.3 eV. In the case of O 1s and N 1s, full width at maximum (FWHM) was set at the same value for each component.

Based on the deconvolution of C 1s, O 1s, and N 1s signals, it can be observed that the obtained AC series contain mainly C-C (sp^3 and sp^2 hybridization) and C-O bonds.

The exception is sample AC, which also contains COOH groups. However, after activation processes, COOH groups decomposed into C=O and C-O bonds. It is assumed that the high concentration of COOH groups is associated with maleic acid, used as a catalyst during polycondensation reactions to prepare the precursor.

In the case of carbons derived from doped-precursors, the addition of NH_4NO_3 caused a substantial increase in the content of C=O groups and a decrease of C-O groups. In the case of the NH_4ClO_4 series, it led to lower concentrations of C=O groups in comparison to the AC series and NH_4NO_3 series. On the other hand, the NH_4ClO_4 -activated carbons are characterized by higher C-O groups concentration than the NH_4NO_3 -activated carbons.

In the case of nitrogen functional groups, NH_4NO_3 - and NH_4ClO_4 -modified activated carbons contain mainly pyridinic (N-6) and nitrogen oxide (N-O) groups. Quaternary nitrogen (N-Q) only appears in samples prepared by carbonization.

Moreover, NH_4NO_3 -activated carbons contain pyrrolic nitrogen (N-5), which is not present in NH_4ClO_4 -activated carbons. Focusing on the quaternary nitrogen concentration, in the NH_4NO_3 series it is higher than in the NH_4ClO_4 series.

3.4. Thermal Stability

Figure 7 compiles the DTG data for either samples obtained after carbonization or after carbonization and activation for 1 h.

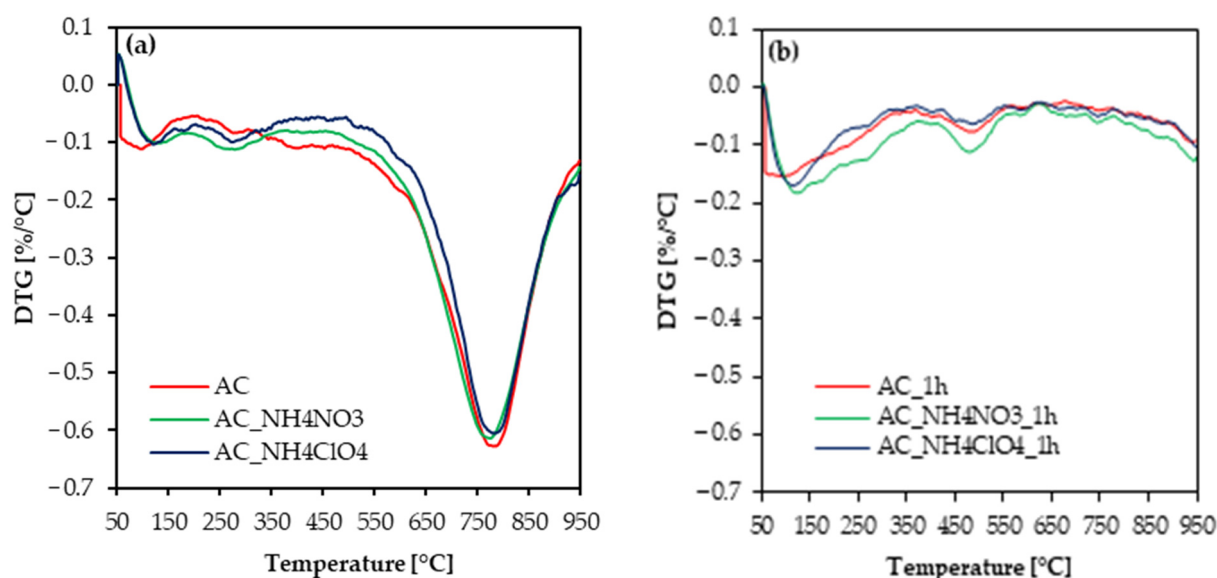


Figure 7. DTG data for determining thermal stability for (a) carbons only after carbonization, (b) carbons after 1 h activation.

In the samples carbonized at 600 °C two peaks, attributed to the removal of volatile organic compounds and adsorbed moisture, appear at low temperatures. The third peak, appearing between 550 °C and 780 °C, helps to understand the stability temperature of the carbonized activated carbons. The DTG data shows that after 1 h activation process, activated carbons have comparable thermal stabilities. Thus, the addition of the NH_4NO_3 or NH_4ClO_4 during the synthesis of the precursor does not modify the thermal stability of the obtained samples.

It is worth highlighting that these loss peaks correspond to the COOH groups removal, which is confirmed by the XPS analysis.

3.5. CO₂ and C₂H₄ Adsorption

CO₂ and C₂H₄ sorption capacities were measured at a temperature of 30 °C. In Figure 8, these capacities are presented.

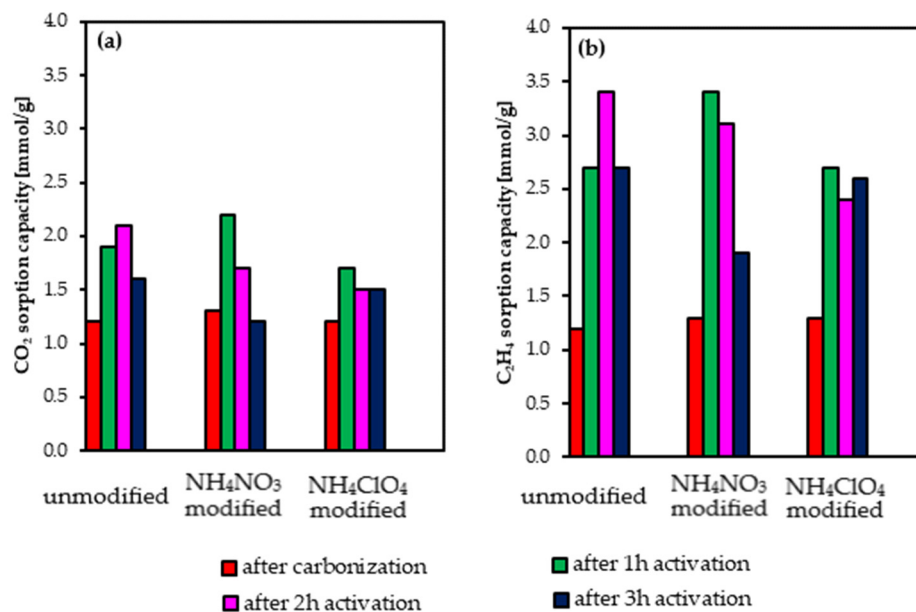


Figure 8. CO₂ (a) and (b) C₂H₄ uptakes at 30 °C.

Figure 8 shows that for all the activated carbons, the C₂H₄ sorption capacity is substantially higher than of CO₂. The carbonized materials show similar and lower CO₂ and C₂H₄ uptakes (~1.3 mmol/g). The highest adsorption of CO₂ was exhibited by the sample AC_NH₄NO₃_1h (2.2 mmol/g). In the unmodified AC series, the highest sorption capacity of CO₂ was exhibited by the sample AC_2h (2.1 mmol/g). So, the incorporation of NH₄NO₃ to the precursor has led to an increase in the sorption properties. The highest C₂H₄ adsorption was reached by the samples AC_2h and AC_NH₄NO₃_1h. It was 3.4 mmol/g.

These results highlight that the incorporation of NH₄NO₃ into the composition of the precursor permits to shorten the activation time: it leads to optimized materials towards CO₂ and C₂H₄ sorption with just 1 h activation time (comparable CO₂ and C₂H₄ sorption capacities are attained from non-doped precursor-activated carbon after 2 h activation).

Figure 8a,b show that the increase in the activation time beyond 2 h for the AC series and beyond 1 h for the NH₄NO₃ and NH₄ClO₄ series leads to a decrease in their sorption capacities of CO₂ and C₂H₄. Comparison of these results with the characterization data of the different activated carbons highlight that porosity, particularly narrow microporosity, seems to be the property determining the CO₂ and C₂H₄ sorption capacities.

Note that the CO₂ and C₂H₄ sorption capacities for the prepared ACs are similar to those from the literature for biomass-derived activated carbons. For instance, Zhang and co-workers produced carbon adsorbents from soybean straw via pyrolysis at 500 °C followed by CO₂ activation at 900 °C [71]. As a result, CO₂ uptake at 30 °C reached 1.5 mmol/g.

Xiong et al. prepared activated carbons from cotton stalks by CO₂ activation at 900 °C [72]. The achieved sorption capacity of CO₂ at 20 °C was 1.8 mmol/g.

On the other hand, Lahijani proposed the preparation of activated carbons from walnut shells via pyrolysis at 900 °C and modification with magnesium [73]. In their case, CO₂ uptake at 25 °C reached 1.9 mmol/g.

Wang et al. obtained carbonaceous materials for the C₂H₄ adsorption using hardwood ligninosulfate as a precursor [74]. The highest C₂H₄ uptake was reached by the sample obtained after pyrolysis at 800 °C. It was 2.2 mmol/g at 25 °C. Ye and co-workers measured the sorption capacities of C₂H₄ and propylene (C₃H₆) for 15 commercial activated carbons [75]. In the case of C₂H₄, the highest uptake was 3.1 mmol/g.

4. Conclusions

The purpose of this study was to examine the influence of NH_4NO_3 and NH_4ClO_4 added during the preparation of a furfuryl-derived precursor on the preparation of ACs by “carbonization” followed by CO_2 activation. It has been shown that the addition of NH_4NO_3 to the precursor’s composition has led to an important porosity enhancement, with specific surface areas up to $1523 \text{ m}^2/\text{g}$, micropore volumes up to $0.41 \text{ cm}^3/\text{g}$, mesopore volumes up to $0.29 \text{ cm}^3/\text{g}$ (and some slight increase in narrow microporosity for a low activation time).

The incorporation of NH_4NO_3 and NH_4ClO_4 does not influence the thermal stability of the prepared carbons but modifies the composition of the surface groups. Thus, an advantage of these modified ACs is that they present surface nitrogen contents between 2–4 at. % and they maintain high surface oxygen contents. The type and contribution of nitrogen species are dependent on the preparation conditions. Quaternary nitrogen only appears in doped samples prepared by carbonization, being larger for NH_4NO_3 . NH_4NO_3 -activated carbons contain pyrrolic nitrogen, not present in NH_4ClO_4 -activated carbon, and both NH_4NO_3 - and NH_4ClO_4 -modified activated carbons contain pyridinic and nitrogen oxide groups.

The prepared ACs present a good structural order, derived from the corresponding carbonized materials. Comparing the influence of the doping salts, carbons in NH_4NO_3 series are characterized by a more disordered structure than from the NH_4ClO_4 series, presenting both series of samples higher disordered structure than the one prepared from the undoped polymer.

The highest adsorption of CO_2 was exhibited by the sample AC- NH_4NO_3 -1h (2.2 mmol/g). In the unmodified AC series, the highest sorption capacity of CO_2 was exhibited by the sample AC-2h (2.1 mmol/g). The highest C_2H_4 adsorption was reached by the samples AC-2h and AC- NH_4NO_3 -1h. It was 3.4 mmol/g . These two ACs present the largest amount of micropores with a mean diameter of around 0.5–0.7 nm, particularly interesting for these applications.

NH_4NO_3 is commonly used as a fertilizer and its cost is relatively low. The precursor’s modification with NH_4NO_3 reduces the activation time from 2 h to 1 h, with the consequent reduction of the production costs, leading to activated carbons with comparable sorption capacities of CO_2 and C_2H_4 to carbons derived from undoped precursors.

Author Contributions: Conceptualization, A.K. and R.J.W.; methodology, A.K., R.J.W., M.C.R.-M. and M.A.L.-R.; validation, A.K., R.J.W. and M.C.R.-M.; investigation, A.K. and R.J.W.; resources, A.K. and R.J.W.; writing—original draft preparation, A.K.; writing—review and editing, R.J.W., M.C.R.-M. and M.A.L.-R.; visualization, A.K. and R.J.W.; supervision, R.J.W., M.C.R.-M. and M.A.L.-R.; project administration, A.K. and R.J.W.; funding acquisition, A.K. All authors have read and agreed to the published version of the manuscript.

Funding: This research was funded by Rector of the West Pomeranian University of Technology in Szczecin for Ph.D. students of the Doctoral School, grant number ZUT/23/2022.

Institutional Review Board Statement: Not applicable.

Informed Consent Statement: Not applicable.

Data Availability Statement: The data presented in this article will be available upon request.

Conflicts of Interest: The authors declare no conflict of interest.

Sample Availability: Samples of the compounds are available in limited amount from the author.

References

1. Alahabadi, A.; Singh, P.; Raizada, P.; Anastopoulos, I.; Sivamani, S.; Dotto, G.L.; Landarani, M.; Ivanets, A.; Kyzas, G.Z.; Hosseini-Bandegharaei, A. Activated Carbon from Wood Wastes for the Removal of Uranium and Thorium Ions through Modification with Mineral Acid. *Colloids Surf. A Physicochem. Eng. Asp.* **2020**, *607*, 125516. [[CrossRef](#)]
2. Danish, M.; Ahmad, T. A Review on Utilization of Wood Biomass as a Sustainable Precursor for Activated Carbon Production and Application. *Renew. Sustain. Energy Rev.* **2018**, *87*, 1–21. [[CrossRef](#)]

3. Asrat, Y.; Adugna, A.T.; Kamaraj, M.; Beyan, S.M. Adsorption Phenomenon of Arundinaria Alpina Stem-Based Activated Carbon for the Removal of Lead from Aqueous Solution. *J. Chem.* **2021**, *2021*, 5554353. [[CrossRef](#)]
4. Ali, I.; Afshinb, S.; Poureshgh, Y.; Azari, A.; Rashtbari, Y.; Feizizadeh, A.; Hamzezadeh, A.; Fazlzadeh, M. Green Preparation of Activated Carbon from Pomegranate Peel Coated with Zero-Valent Iron Nanoparticles (NZVI) and Isotherm and Kinetic Studies of Amoxicillin Removal in Water. *Environ. Sci. Pollut. Res.* **2020**, *27*, 36732–36743. [[CrossRef](#)]
5. Foo, K.Y.; Hameed, B.H. Preparation, Characterization and Evaluation of Adsorptive Properties of Orange Peel Based Activated Carbon via Microwave Induced K₂CO₃ Activation. *Bioresour. Technol.* **2012**, *104*, 679–686. [[CrossRef](#)] [[PubMed](#)]
6. Huang, G.; Liu, Y.; Wu, X.; Cai, J. Activated Carbons Prepared by the KOH Activation of a Hydrochar from Garlic Peel and Their CO₂ Adsorption Performance. *New Carbon Mater.* **2019**, *34*, 247–257. [[CrossRef](#)]
7. Zheng, L.; Wang, S.; Yang, Y.; Fu, X.; Jiang, T.; Yang, J. Ammonium Nitrate-Assisted Synthesis of Nitrogen/Sulfur-Codoped Hierarchically Porous Carbons Derived from Ginkgo Leaf for Supercapacitors. *ACS Omega* **2019**, *4*, 5904–5914. [[CrossRef](#)]
8. Lucas, W.J.; Groover, A.; Lichtenberger, R.; Furuta, K.; Yadav, S.-R.; Helariutta, Y.; He, X.-Q.; Fukuda, H.; Kang, J.; Brady, S.M.; et al. The Plant Vascular System: Evolution, Development and Functions. *J. Integr. Plant Biol.* **2013**, *55*, 294–388. [[CrossRef](#)] [[PubMed](#)]
9. Matsuzawa, F.; Amano, Y.; Machida, M. Phosphate Ion Adsorption Characteristics of PAN-Based Activated Carbon Prepared by Zinc Chloride Activation. *Int. J. Environ. Sci. Technol.* **2022**, *19*, 8159–8168. [[CrossRef](#)]
10. László, K.; Szűcs, A. Surface Characterization of Polyethyleneterephthalate (PET) Based Activated Carbon and the Effect of PH on Its Adsorption Capacity from Aqueous Phenol and 2,3,4-Trichlorophenol Solutions. *Carbon* **2001**, *39*, 1945–1953. [[CrossRef](#)]
11. Alcañiz-Monge, J.; Román-Martínez, M.d.C.; Lillo-Ródenas, M.Á. Chemical Activation of Lignocellulosic Precursors and Residues: What Else to Consider? *Molecules* **2022**, *27*, 1630. [[CrossRef](#)] [[PubMed](#)]
12. Hu, S.; Jiang, L.; Wang, Y.; Su, S.; Sun, L.; Xu, B.; He, L.; Xiang, J. Effects of Inherent Alkali and Alkaline Earth Metallic Species on Biomass Pyrolysis at Different Temperatures. *Bioresour. Technol.* **2015**, *192*, 23–30. [[CrossRef](#)] [[PubMed](#)]
13. Zhou, L.; Zhang, G.; Reinmüller, M.; Meyer, B. Effect of Inherent Mineral Matter on the Co-Pyrolysis of Highly Reactive Brown Coal and Wheat Straw. *Fuel* **2019**, *239*, 1194–1203. [[CrossRef](#)]
14. Gesikiewicz-Puchalska, A.; Zgrzebnicki, M.; Michalkiewicz, B.; Narkiewicz, U.; Morawski, A.W.; Wrobel, R.J. Improvement of CO₂ Uptake of Activated Carbons by Treatment with Mineral Acids. *Chem. Eng. J.* **2017**, *309*, 159–171. [[CrossRef](#)]
15. Zhang, Y.; Song, X.; Zhang, P.; Gao, H.; Ou, C.; Kong, X. Production of Activated Carbons from Four Wastes via One-Step Activation and Their Applications in Pb²⁺ Adsorption: Insight of Ash Content. *Chemosphere* **2020**, *245*, 125587. [[CrossRef](#)]
16. Zhang, X.-Y.; Xu, Z.-H.; Zong, M.-H.; Wang, C.-F.; Li, N. Selective Synthesis of Furfuryl Alcohol from Biomass-Derived Furfural Using Immobilized Yeast Cells. *Catalysts* **2019**, *9*, 70. [[CrossRef](#)]
17. Cao Nhien, L.; Van Duc Long, N.; Kim, S.; Lee, M. Novel Reaction-Hybrid-Extraction-Distillation Process for Furfuryl Alcohol Production from Raw Bio-Furfural. *Biochem. Eng. J.* **2019**, *148*, 143–151. [[CrossRef](#)]
18. Principe, M.; Martínez, R.; Ortiz, P.; Rieumont, J. The Polymerization of Furfuryl Alcohol with P-Toluenesulfonic Acid: Photocross-Linkable Feature of the Polymer. *Polímeros* **2000**, *10*, 08–14. [[CrossRef](#)]
19. Dubinsky, J.; Žagars, A.; Snidvongs, S.; Hirunlabh, J. Furfuryl Alcohol Made from Agriculture Waste Review. In Proceedings of the Fourth National and the Third International Academic Symposium Innovation and Technology for Social Development, Bangkok, Thailand, 23 July 2018.
20. Arnaiz, M.; Nair, V.; Mitra, S.; Ajuria, J. Furfuryl Alcohol Derived High-End Carbons for Ultrafast Dual Carbon Lithium Ion Capacitors. *Electrochim. Acta* **2019**, *304*, 437–446. [[CrossRef](#)]
21. Zgrzebnicki, M.; Nair, V.; Mitra, S.; Kalamaga, A.; Przepiórski, J.; Wrobel, R.J. N-Doped Activated Carbon Derived from Furfuryl Alcohol—Development of Porosity, Properties, and Adsorption of Carbon Dioxide and Ethene. *Chem. Eng. J.* **2022**, *427*, 131709. [[CrossRef](#)]
22. Jiang, C.; Yakaboylu, G.A.; Yumak, T.; Zondlo, J.W.; Sabolsky, E.M.; Wang, J. Activated Carbons Prepared by Indirect and Direct CO₂ Activation of Lignocellulosic Biomass for Supercapacitor Electrodes. *Renew. Energy* **2020**, *155*, 38–52. [[CrossRef](#)]
23. Ouyang, J.; Zhou, L.; Liu, Z.; Heng, J.Y.Y.; Chen, W. Biomass-Derived Activated Carbons for the Removal of Pharmaceutical Mircopollutants from Wastewater: A Review. *Sep. Purif. Technol.* **2020**, *253*, 117536. [[CrossRef](#)]
24. Moreno-Castilla, C.; Carrasco-Marín, F.; Lopez-Ramon, M.V.; Alvarez-Merino, M.A. Chemical and Physical Activation of Olive-Mill Waste Water to Produce Activated Carbons. *Carbon* **2001**, *39*, 1415–1420. [[CrossRef](#)]
25. Şahin, Ö.; Saka, C. Preparation and Characterization of Activated Carbon from Acorn Shell by Physical Activation with H₂O–CO₂ in Two-Step Pretreatment. *Bioresour. Technol.* **2013**, *136*, 163–168. [[CrossRef](#)]
26. Hassan, M.F.; Sabri, M.A.; Fazal, H.; Hafeez, A.; Shezad, N.; Hussain, M. Recent Trends in Activated Carbon Fibers Production from Various Precursors and Applications—A Comparative Review. *J. Anal. Appl. Pyrolysis* **2020**, *145*, 104715. [[CrossRef](#)]
27. Jjagwe, J.; Olupot, P.W.; Menya, E.; Kalibbala, H.M. Synthesis and Application of Granular Activated Carbon from Biomass Waste Materials for Water Treatment: A Review. *J. Bioresour. Bioprod.* **2021**, *6*, 292–322. [[CrossRef](#)]
28. Kosheleva, R.I.; Mitropoulos, A.C.; Kyzas, G.Z. Synthesis of Activated Carbon from Food Waste. *Environ. Chem. Lett.* **2019**, *17*, 429–438. [[CrossRef](#)]
29. Heidarinejad, Z.; Dehghani, M.H.; Heidari, M.; Javedan, G.; Ali, I.; Sillanpää, M. Methods for Preparation and Activation of Activated Carbon: A Review. *Environ. Chem. Lett.* **2020**, *18*, 393–415. [[CrossRef](#)]
30. Rashidi, N.A.; Yusup, S. Production of Palm Kernel Shell-Based Activated Carbon by Direct Physical Activation for Carbon Dioxide Adsorption. *Environ. Sci. Pollut. Res.* **2019**, *26*, 33732–33746. [[CrossRef](#)]

31. Olivares-Marín, M.; Fernández-González, C.; Macías-García, A.; Gómez-Serrano, V. Preparation of Activated Carbon from Cherry Stones by Physical Activation in Air. Influence of the Chemical Carbonisation with H₂SO₄. *J. Anal. Appl. Pyrolysis* **2012**, *94*, 131–137. [[CrossRef](#)]
32. Rodríguez-Reinoso, F.; Molina-Sabio, M.; Gonzalez, M.T. The use of steam and CO₂ as activating agents in the preparation of activated carbons. *Carbon* **1995**, *33*, 15–23. [[CrossRef](#)]
33. Ao, W.; Fu, J.; Mao, X.; Kang, Q.; Ran, C.; Liu, Y.; Zhang, H.; Gao, Z.; Li, J.; Liu, G.; et al. Microwave Assisted Preparation of Activated Carbon from Biomass: A Review. *Renew. Sustain. Energy Rev.* **2018**, *92*, 958–979. [[CrossRef](#)]
34. Liew, R.K.; Azwar, E.; Yek, P.N.Y.; Lim, X.Y.; Cheng, C.K.; Ng, J.-H.; Jusoh, A.; Lam, W.H.; Ibrahim, M.D.; Ma, N.L.; et al. Microwave Pyrolysis with KOH/NaOH Mixture Activation: A New Approach to Produce Micro-Mesoporous Activated Carbon for Textile Dye Adsorption. *Bioresour. Technol.* **2018**, *266*, 1–10. [[CrossRef](#)] [[PubMed](#)]
35. Lee, D.Y.; Choi, J.H.; Shin, J.C.; Jung, M.K.; Song, S.K.; Suh, J.K.; Lee, C.Y. Plasma Functionalization of Powdery Nanomaterials Using Porous Filter Electrode and Sample Circulation. *Appl. Surf. Sci.* **2018**, *443*, 628–634. [[CrossRef](#)]
36. Ortiz-Ortega, E.; Hosseini, S.; Martinez-Chapa, S.O.; Madou, M.J. Aging of Plasma-Activated Carbon Surfaces: Challenges and Opportunities. *Appl. Surf. Sci.* **2021**, *565*, 150362. [[CrossRef](#)]
37. Zhang, W.; Yang, P.; Luo, M.; Wang, X.; Zhang, T.; Chen, W.; Zhou, X. Fast Oxygen, Nitrogen Co-Functionalization on Electrospun Lignin-Based Carbon Nanofibers Membrane via Air Plasma for Energy Storage Application. *Int. J. Biol. Macromol.* **2020**, *143*, 434–442. [[CrossRef](#)]
38. Chen, W.; Gong, M.; Li, K.; Xia, M.; Chen, Z.; Xiao, H.; Fang, Y.; Chen, Y.; Yang, H.; Chen, H. Insight into KOH Activation Mechanism during Biomass Pyrolysis: Chemical Reactions between O-Containing Groups and KOH. *Appl. Energy* **2020**, *278*, 115730. [[CrossRef](#)]
39. Li, S.; Han, K.; Li, J.; Li, M.; Lu, C. Preparation and Characterization of Super Activated Carbon Produced from Gulfweed by KOH Activation. *Microporous Mesoporous Mater.* **2017**, *243*, 291–300. [[CrossRef](#)]
40. Sevilla, M.; Ferrero, G.A.; Fuertes, A.B. Beyond KOH Activation for the Synthesis of Superactivated Carbons from Hydrochar. *Carbon* **2017**, *114*, 50–58. [[CrossRef](#)]
41. Muniandy, L.; Adam, F.; Mohamed, A.R.; Ng, E.-P. The Synthesis and Characterization of High Purity Mixed Microporous/Mesoporous Activated Carbon from Rice Husk Using Chemical Activation with NaOH and KOH. *Microporous Mesoporous Mater.* **2014**, *197*, 316–323. [[CrossRef](#)]
42. Singh, J.; Bhunia, H.; Basu, S. Adsorption of CO₂ on KOH Activated Carbon Adsorbents: Effect of Different Mass Ratios. *J. Environ. Manag.* **2019**, *250*, 109457. [[CrossRef](#)] [[PubMed](#)]
43. Le Van, K.; Luong Thi, T.T. Activated Carbon Derived from Rice Husk by NaOH Activation and Its Application in Supercapacitor. *Progress Nat. Sci. Mater. Int.* **2014**, *24*, 191–198. [[CrossRef](#)]
44. Xu, B.; Chen, Y.; Wei, G.; Cao, G.; Zhang, H.; Yang, Y. Activated Carbon with High Capacitance Prepared by NaOH Activation for Supercapacitors. *Mater. Chem. Phys.* **2010**, *124*, 504–509. [[CrossRef](#)]
45. Liu, J.; Yang, X.; Liu, H.; Cheng, W.; Bao, Y. Modification of Calcium-Rich Biochar by Loading Si/Mn Binary Oxide after NaOH Activation and Its Adsorption Mechanisms for Removal of Cu(II) from Aqueous Solution. *Colloids Surf. A Physicochem. Eng. Asp.* **2020**, *601*, 124960. [[CrossRef](#)]
46. Dawei, L.; Yu, W.; Jiaojiao, Z.; Jicheng, W.; Xiaoyang, L.; Yuanyu, T.; Zongbo, Z.; Yingyun, Q.; Ling, W.; Junhua, L.; et al. Drying before Microwave-Assisted H₃PO₄ Activation to Produce Highly Mesoporous Activated Carbons. *Mater. Lett.* **2018**, *230*, 61–63. [[CrossRef](#)]
47. Yang, Z.; Gleisner, R.; Mann, D.H.; Xu, J.; Jiang, J.; Zhu, J.Y. Lignin Based Activated Carbon Using H₃PO₄ Activation. *Polymers* **2020**, *12*, 2829. [[CrossRef](#)]
48. Jawad, A.H.; Malek, N.N.A.; Khadiran, T.; AlOthman, Z.A.; Yaseen, Z.M. Mesoporous High-Surface-Area Activated Carbon from Biomass Waste via Microwave-Assisted-H₃PO₄ Activation for Methylene Blue Dye Adsorption: An Optimized Process. *Diam. Relat. Mater.* **2022**, *128*, 109288. [[CrossRef](#)]
49. Vunain, E.; Njewa, J.B.; Biswick, T.T.; Ipadeola, A.K. Adsorption of Chromium Ions from Tannery Effluents onto Activated Carbon Prepared from Rice Husk and Potato Peel by H₃PO₄ Activation. *Appl. Water Sci.* **2021**, *11*, 150. [[CrossRef](#)]
50. Uçar, S.; Erdem, M.; Tay, T.; Karagöz, S. Preparation and Characterization of Activated Carbon Produced from Pomegranate Seeds by ZnCl₂ Activation. *Appl. Surf. Sci.* **2009**, *255*, 8890–8896. [[CrossRef](#)]
51. Nakagawa, Y.; Molina-Sabio, M.; Rodríguez-Reinoso, F. Modification of the Porous Structure along the Preparation of Activated Carbon Monoliths with H₃PO₄ and ZnCl₂. *Microporous Mesoporous Mater.* **2007**, *103*, 29–34. [[CrossRef](#)]
52. Wang, T.; Tan, S.; Liang, C. Preparation and Characterization of Activated Carbon from Wood via Microwave-Induced ZnCl₂ Activation. *Carbon* **2009**, *47*, 1880–1883. [[CrossRef](#)]
53. Sakamoto, T.; Amano, Y.; Machida, M. Phosphate Ion Adsorption Properties of PAN-Based Activated Carbon Fibers Prepared with K₂CO₃ Activation. *SN Appl. Sci.* **2020**, *2*, 702. [[CrossRef](#)]
54. Sajjadi, S.-A.; Mohammadzadeh, A.; Tran, H.N.; Anastopoulos, I.; Dotto, G.L.; Lopičić, Z.R.; Sivamani, S.; Rahmani-Sani, A.; Ivanets, A.; Hosseini-Bandegharai, A. Efficient Mercury Removal from Wastewater by Pistachio Wood Wastes-Derived Activated Carbon Prepared by Chemical Activation Using a Novel Activating Agent. *J. Environ. Manag.* **2018**, *223*, 1001–1009. [[CrossRef](#)]
55. Fu, K.; Yue, Q.; Gao, B.; Wang, Y.; Li, Q. Activated Carbon from Tomato Stem by Chemical Activation with FeCl₂. *Colloids Surf. A Physicochem. Eng. Asp.* **2017**, *529*, 842–849. [[CrossRef](#)]
56. Subramanian, N.; Viswanathan, B. Nitrogen- and Oxygen-Containing Activated Carbons from Sucrose for Electrochemical Supercapacitor Applications. *RSC Adv.* **2015**, *5*, 63000–63011. [[CrossRef](#)]

57. Bayrak, Y.; Topallar, H.; Karagöz, B.; Kılıç, İ. Kinetics and Thermodynamics of Cr(VI), Cu(II), and Ni(II) Adsorption on Activated Carbon Prepared from Rice Hulls. *J. Dispers. Sci. Technol.* **2013**, *34*, 1248–1256. [[CrossRef](#)]
58. Sajjadi, S.-A.; Meknati, A.; Lima, E.C.; Dotto, G.L.; Mendoza-Castillo, D.I.; Anastopoulos, I.; Alakhras, F.; Unuabonah, E.I.; Singh, P.; Hosseini-Bandegharaei, A. A Novel Route for Preparation of Chemically Activated Carbon from Pistachio Wood for Highly Efficient Pb(II) Sorption. *J. Environ. Manag.* **2019**, *236*, 34–44. [[CrossRef](#)]
59. Ma, X.-Q.; Zhang, B.; Xu, Z.-X.; Tan, Y.; Li, B.; Zhang, Y.-C.; Ni, G.-S.; Zhou, W.-Y.; Luque, R.; Zhang, H.-Y. N-Rich and O-Poor Doped Carbon Prepared via Facile Ammonium Nitrate Assisted Hydrothermal Carbonization for Robust Supercapacitors. *J. Clean. Prod.* **2022**, *373*, 133903. [[CrossRef](#)]
60. Boldyrev, V.V. Thermal Decomposition of Ammonium Perchlorate. *Thermochim. Acta* **2006**, *443*, 1–36. [[CrossRef](#)]
61. Sharma, J.K.; Srivastava, P.; Singh, G.; Akhtar, M.S.; Ameen, S. Catalytic Thermal Decomposition of Ammonium Perchlorate and Combustion of Composite Solid Propellants over Green Synthesized CuO Nanoparticles. *Thermochim. Acta* **2015**, *614*, 110–115. [[CrossRef](#)]
62. Xie, Y.; Wang, Y.; Giammar, D.E. Impact of Chlorine Disinfectants on Dissolution of the Lead Corrosion Product PbO₂. *Environ. Sci. Technol.* **2010**, *44*, 7082–7088. [[CrossRef](#)] [[PubMed](#)]
63. Raza, A.; Gholami, R.; Rezaee, R.; Rasouli, V.; Rabiei, M. Significant Aspects of Carbon Capture and Storage—A Review. *Petroleum* **2019**, *5*, 335–340. [[CrossRef](#)]
64. Chen, Y.; Grimplet, J.; David, K.; Castellarin, S.D.; Terol, J.; Wong, D.C.J.; Luo, Z.; Schaffer, R.; Celton, J.-M.; Talon, M.; et al. Ethylene Receptors and Related Proteins in Climacteric and Non-Climacteric Fruits. *Plant Sci.* **2018**, *276*, 63–72. [[CrossRef](#)] [[PubMed](#)]
65. Thommes, M.; Kaneko, K.; Neimark, A.V.; Olivier, J.P.; Rodriguez-Reinoso, F.; Rouquerol, J.; Sing, K.S.W. Physisorption of Gases, with Special Reference to the Evaluation of Surface Area and Pore Size Distribution (IUPAC Technical Report). *Pure Appl. Chem.* **2015**, *87*, 1051–1069. [[CrossRef](#)]
66. Puech, P.; Dabrowska, A.; Ratel-Ramond, N.; Vignoles, G.L.; Monthieux, M. New Insight on Carbonisation and Graphitisation Mechanisms as Obtained from a Bottom-up Analytical Approach of X-Ray Diffraction Patterns. *Carbon* **2019**, *147*, 602–611. [[CrossRef](#)]
67. Fujimoto, H. Theoretical X-Ray Scattering Intensity of Carbons with Turbostratic Stacking and AB Stacking Structures. *Carbon* **2003**, *41*, 1585–1592. [[CrossRef](#)]
68. Cañado, L.G.; Takai, K.; Enoki, T.; Endo, M.; Kim, Y.A.; Mizusaki, H.; Jorio, A.; Coelho, L.N.; Magalhães-Paniago, R.; Pimenta, M.A. General Equation for the Determination of the Crystallite Size La of Nanographite by Raman Spectroscopy. *Appl. Phys. Lett.* **2006**, *88*, 163106. [[CrossRef](#)]
69. Zhao, Z.; Dai, Y.; Ge, G. Nitrogen-Doped Nanotubes-Decorated Activated Carbon-Based Hybrid Nanoarchitecture as a Superior Catalyst for Direct Dehydrogenation. *Catal. Sci. Technol.* **2015**, *5*, 1548–1557. [[CrossRef](#)]
70. Kumar, N.; Srivastava, V.C. Simple Synthesis of Large Graphene Oxide Sheets via Electrochemical Method Coupled with Oxidation Process. *ACS Omega* **2018**, *3*, 10233–10242. [[CrossRef](#)]
71. Zhang, X.; Wu, J.; Yang, H.; Shao, J.; Wang, X.; Chen, Y.; Zhang, S.; Chen, H. Preparation of Nitrogen-Doped Microporous Modified Biochar by High Temperature CO₂-NH₃ Treatment for CO₂ Adsorption: Effects of Temperature. *RSC Adv.* **2016**, *6*, 98157–98166. [[CrossRef](#)]
72. Xiong, Z.; Shihong, Z.; Haiping, Y.; Tao, S.; Yingquan, C.; Hanping, C. Influence of NH₃/CO₂ Modification on the Characteristic of Biochar and the CO₂ Capture. *Bioenerg. Res.* **2013**, *6*, 1147–1153. [[CrossRef](#)]
73. Lahijani, P.; Mohammadi, M.; Mohamed, A.R. Metal Incorporated Biochar as a Potential Adsorbent for High Capacity CO₂ Capture at Ambient Condition. *J. CO₂ Util.* **2018**, *26*, 281–293. [[CrossRef](#)]
74. Wang, S.-H.; Hwang, Y.-K.; Choi, S.W.; Yuan, X.; Lee, K.B.; Chang, F.-C. Developing Self-Activated Lignosulfonate-Based Porous Carbon Material for Ethylene Adsorption. *J. Taiwan Inst. Chem. Eng.* **2020**, *115*, 315–320. [[CrossRef](#)]
75. Ye, P.; Fang, Z.; Su, B.; Xing, H.; Yang, Y.; Su, Y.; Ren, Q. Adsorption of Propylene and Ethylene on 15 Activated Carbons. *J. Chem. Eng. Data* **2010**, *55*, 5669–5672. [[CrossRef](#)]